Mapping Spin Coherence of a Single Rare-Earth Ion in a Crystal onto a Single Photon Polarization State

Roman Kolesov, Kangwei Xia, Rolf Reuter, Mohammad Jamali,
Rainer Stöhr, Tugrul Inal, Petr Siyushev, and Jörg Wrachtrup

3. Physikalisches Institut, Universität Stuttgart and Stuttgart Research Center of Photonic Engineering (SCoPE), Pfaffenwaldring 57, Stuttgart D-70569, Germany

(Received 10 February 2013; published 20 September 2013)

We report on optical detection of a single photostable Ce^{3+} ion in an yttrium aluminium garnet (YAG) crystal and on its magneto-optical properties at room temperature. The spin quantum state of the emitting level of a single cerium ion in YAG can be initialized by a circularly polarized laser pulse. Coherent precession of the electron spin is read out by observing temporal behavior of circularly polarized fluorescence of the ion. This implies direct mapping of the spin quantum state of Ce^{3+} ion onto the polarization state of the emitted photon and represents the quantum interface between a single spin and a single photon.

DOI: 10.1103/PhysRevLett.111.120502 PACS numbers: 03.67.−a, 42.50.Ex, 76.30.Kg, 78.47.jm

Rare-earth (RE) doped optical materials are known to have outstanding properties for optical information storage and processing, both classical [1,2] and quantum [3,4]. The most valuable features of RE ions are their quantum transitions between electronic and nuclear hyperfine levels having an extremely high quality factor due to efficient screening of optically active $4f$ electrons from the surrounding environment by outer lying $5s$ and $5p$ electronic shells. As a result, RE ions in optical crystals have demonstrated benchmark performance in storing light for over a second [2], storing and retrieving the quantum state at a single photon level [3], and quantum entanglement [4], etc. In these demonstrations, the quantum state of a single flying qubit (a photon) or of a pair of entangled flying qubits is mapped onto an ensemble of RE ions. Other important functionalities like entanglement purification require access to single rare-earth ions. One has to either use optically addressable single RE spins as stationary qubits or exploit the emission of a single RE ion to read out the state of other RE species possessing favorable spin properties, e.g., long decoherence times, but having too low photon yield for direct readout [5]. In either case, optical addressability of RE species at the single ion level is an absolute prerequisite for incorporation of the outstanding properties of RE-based memories in quantum data processing. However, the high Q factor of the $4f \leftrightarrow 4f$ electronic transitions of RE ions inevitably results in very low photon flux emitted by an individual ion. This makes single RE ions in crystals very hard to detect by observing their emission at high-Q transitions. Only recently, two successful attempts of detecting individual RE ions, namely, Pr^{3+} in yttrium aluminium garnet (YAG) and Er^{3+} in silicon, were reported [6,7].

In this work, we optically address for the first time single electron spins of Ce^{3+} ions in a crystal. We show that the electron spin of an ion can be prepared in a coherent state by circularly polarized laser excitation. Furthermore, spin coherence can be efficiently mapped onto the polarization state of a photon emitted by a Ce^{3+} ion, demonstrating a coherent interface between a single spin and a single photon.

Ce^{3+}:YAG is an efficient scintillator with peak emission at ≈ 550 nm and quite short lifetime (~ 60 ns). The fluorescence of Ce^{3+} can be efficiently excited by optical pumping with 460 nm radiation into the phonon absorption sideband of the lowest $5d$ level. With almost unity quantum efficiency of the optical transition [8], a single Ce^{3+} ion is expected to emit 1.6×10^7 photons per second. Such photon flux can be easily detected by means of confocal microscopy. To distinguish individual ions in a crystal, the distance between them should be greater than the resolution of the microscope. The latter cannot be better than a half wavelength of the excitation radiation in the YAG crystal, $460\ \text{nm}/2/1.82 = 126$ nm (here 1.82 is the refractive index of YAG), resulting in a maximum cerium concentration of 36 ppb (parts per billion) relative to yttrium. This value sets the absolute upper limit on the concentration of cerium impurity. However, any yttrium-based crystal contains trace amounts of all RE elements, so that only the crystals of highest purity can be used for isolation of a single emitting ion.

In our study, we used the same crystal in which single praseodymium ions were detected [6] (ultrapure YAG crystal from Scientific Materials). Optical detection of a single cerium center was performed in a home-built confocal microscope operating at room temperature (see the Supplemental Material, Fig. S1 [9]). We used frequency-doubled output of a femtosecond Ti:sapphire laser operating at ≈ 920 nm as an excitation source. The repetition rate of excitation pulses was adjusted to a few MHz by a pulse picker. The fluorescence of cerium ions was split into two paths and detected by two single-photon-counting

detectors in order to allow for photon correlation measurements. The detection wavelength range was restricted between 485 and 630 nm to reject the excitation light and to block the fluorescence of the residual Ce^{3+} impurity ions present in the crystal (680 nm). The resulting scanning image of the crystal is shown in Fig. 1(a). Individual bright spots correspond to single cerium ions. This was confirmed by (i) photon correlation measurements performed on these spots showing pronounced antibunching at zero delay time between the clicks on the detectors [see Fig. 1(b)]; (ii) the fluorescence lifetime of each spot is close to 64 ns in agreement with the lifetime data taken on bulk Ce:YAG crystals [see Fig. 1(c)]; (iii) the emission spectrum is the same as that of the bulk Ce:YAG crystals [see Fig. 1(d)]. The typical photon count rate on the two detectors produced by a single Ce^{3+} ion was 40–50 kcounts/s for pulse repetition rate 7.6 MHz corresponding to the detection efficiency of $\approx 0.7\%$ (see the Supplemental Material [9] for a detailed discussion). The ions are absolutely photostable and show no blinking at time scales down to 1 ms.

To get insight into the optically excited spin dynamics of Ce^{3+} in YAG, we consider its electronic energy level structure in detail (see the Supplemental Material [9] for the level structure calculation procedure). The Ce^{3+} ion has only one unpaired electron whose ground state is $4f^1$. The 14-fold degeneracy of that state (sevenfold orbital degeneracy times doubly degenerate spin) is lifted by the combined action of spin-orbit coupling and the crystal field [see Fig. 2(a)]. Overall, the $4f^1$ manifold is split into 7 Kramer's doublets whose degeneracy can be lifted only by an external magnetic field and which are grouped into two submanifolds,

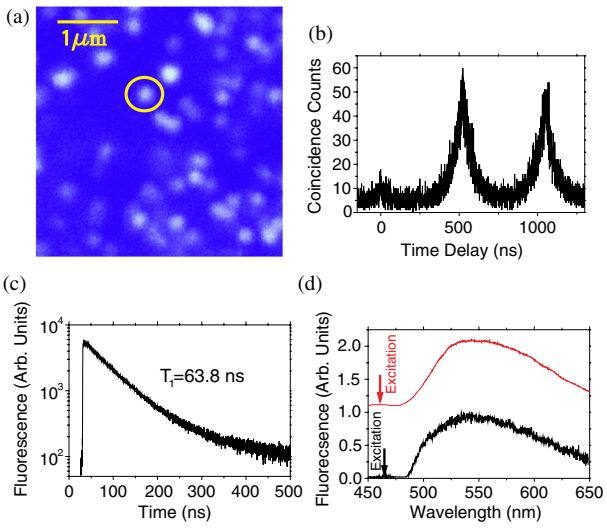

FIG. 1 (color online). Detection of a single Ce^{3+} ion in a YAG crystal. (a) Scanning confocal image of Ce^{3+} centers in a nominally pure YAG crystal. (b) Photon correlation signal taken on the marked spot on (a) with a pulsed laser excitation. Antibunching at zero time delay indicates that the emitter is indeed a single quantum object. (c) Fluorescence decay signal taken on the same spot reveals the lifetime of 64 ns in agreement with the known lifetime of the lowest $5d$ state of Ce^{3+} in YAG. (d) The spectrum of the emission of the same spot (lower curve, black line) well correlates with the fluorescence spectrum of a bulk Ce:YAG crystal (upper curve, red line).

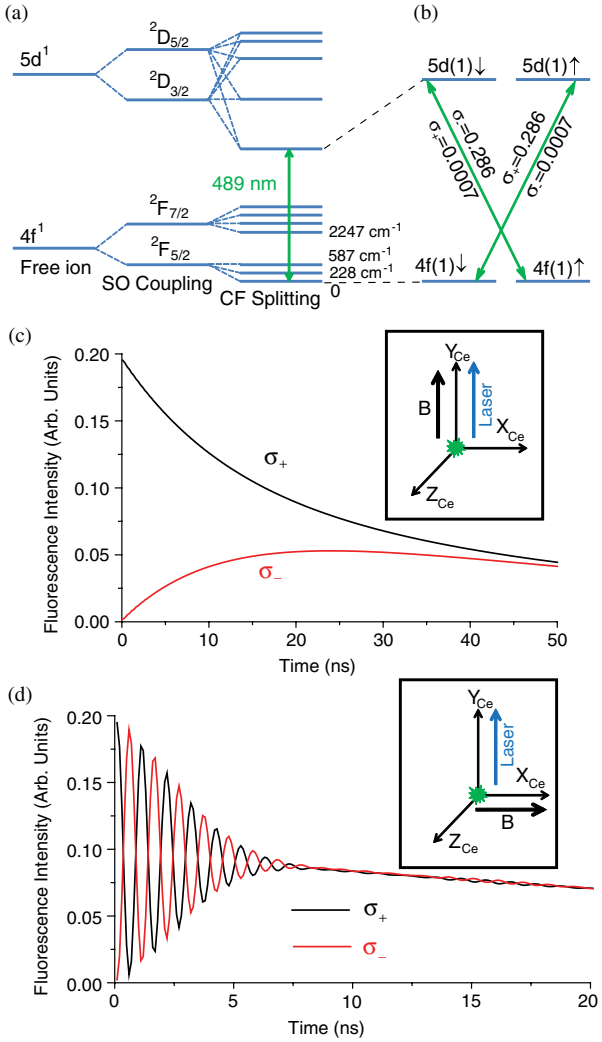

FIG. 2 (color online). Electronic level structure of Ce^{3+} ion in a YAG crystal. (a) $4f^1$ and $5d^1$ shells are split by a combined action of spin-orbit coupling and the crystal field. While in the $4f^1$ state spin-orbit coupling dominates, in the $5d^1$ states the major contribution to the splitting is from the crystal field. (b) Strengths of the transition dipoles between the lowest $4f$ and the lowest $5d$ Kramer's doublets. The quantization axis is chosen along the y axis of the local frame of the cerium site [10]. (c) Calculated time traces of the fluorescence corresponding to the ZPL of Ce^{3+} once the ion is pumped into one of the lowest $5d$ spin sublevels. The magnetic field is along the y axis of the local frame of cerium site. The σ_- polarization (red curve) builds up due to spin relaxation while the σ_+ polarization (black curve) declines until it reaches the level of σ_- polarization. (d) Calculated fluorescence oscillations with the external magnetic field applied along the x axis of the local frame of cerium site. The curves corresponding to σ_+/σ_- start at maximum/minimum, respectively.

$^2F_{5/2}$ and $^2F_{7/2}$, containing 3 and 4 doublets, respectively. The energy difference between $^2F_{5/2}$ and $^2F_{7/2}$ is mostly defined by spin-orbit coupling while the splitting within the manifolds is determined by the crystal field. On the contrary, the structure of the $5d$ electronic levels is dominated by crystal field splitting slightly perturbed by spin-orbit interaction. For the $5d$ levels the electron spin is a good quantum number while in the $4f$ states the spin is highly mixed with the orbital momentum. This suggests that the optical transitions between the $4f$ and the $5d$ levels allow spin flip.

Owing to its spin-flip optical transitions, Ce^{3+}:YAG crystals exhibit a strong Faraday effect [11]. The inverse effect, i.e., magnetizing the material by circularly polarized optical field, was demonstrated by direct measurement of the magnetic moment of Ce:YAG crystal induced by a circularly polarized laser pulse [12]. In this process, the Ce^{3+} spin can be oriented in the $5d(1)$ level by the excitation light and, vice versa, the polarization of the Ce^{3+} fluorescence depends on the spin state of the emitting $5d$ level. Quantitative understanding of this dependence requires the knowledge of the orientations of the dipoles associated with the optical transitions between the $4f$ and the lowest $5d$ Kramer's doublets. The result of a detailed calculation (see the Supplemental Material [9]) is depicted in Fig. 2(b) and in the Supplemental Material, Fig. S2 [9]. Since the ratio of the oscillator strengths of the transitions $|4f(1)\downarrow\rangle \leftrightarrow |5d(1)\uparrow\rangle$ and $|4f(1)\uparrow\rangle \leftrightarrow |5d(1)\downarrow\rangle$ is $0.284/0.0007 \approx 400$ for σ_+/σ_- polarizations, circularly polarized light can excite Ce^{3+} ion from its lowest $4f$ doublet into one of the $5d$ spin states 400 times more efficiently than into the other spin state resulting in almost perfect spin polarization (99.7%) in the excited state. In turn, the emission originating from one of the spin sublevels of the lowest $5d$ state and terminating at the lowest $4f$ doublet [$4f(1)$ in Fig. 2(b)] should be circularly polarized. This transition corresponds to the zero-phonon line (ZPL) of Ce^{3+}:YAG at 489 nm [13]. Any relaxation process leading to spin flip in the $5d$ emitting state results in depolarization of emitted photons as shown in Fig. 2(c).

If an external magnetic field is applied perpendicular to the system quantization axis, $5d(\uparrow)$ and $5d(\downarrow)$ are no longer eigenstates of the system and the excited state spin starts precessing at Larmor frequency defined by the magnitude of the field and the g factor of the $5d(1)$ state $\omega = \mu_B g_\perp B_\perp/\hbar$. This results in a new excited state wave function,

$$|\psi\rangle = \tfrac{1}{2}(|5d(1)\uparrow\rangle + e^{-i\omega t}|5d(1)\downarrow\rangle), \quad (1)$$

which leads to an oscillatory behavior of the σ_+ and σ_- components of the fluorescence [see Fig. 2(d)]. Any decoherence process shortens the lifetime of oscillations. In case of YAG host, dephasing arises from the hyperfine interaction with the surrounding ^{27}Al nuclei producing random magnetic field (≈ 40 G on average [12]) at the location of Ce^{3+}.

To achieve good fidelity in the observation of oscillations between $5d(\uparrow)$ and $5d(\downarrow)$ states it is important to filter the emitted photons spectrally. In particular, the emission terminating at the levels belonging to the $^2F_{5/2}$ manifold can be separated by detecting only the wavelengths shorter than 550 nm since the lowest $^2F_{7/2}$ level is 2250 cm^{-1} above the ground state (see Fig. 2). Under these circumstances, the coherent dynamics of the excited electron spin is detectable even at room temperature, though not with the full contrast. In addition, it depends on the orientation of local Ce^{3+} site with respect to the excitation and detection direction. In our case, the geometry of the crystal allowed excitation only along the (111) direction resulting in significant though not the best polarization of Ce^{3+} spin. The calculated polarized fluorescence signals relevant to our experimental conditions, i.e., room temperature and (111) orientation of the crystal, are shown in the Supplemental Material, Fig. S3 [9].

Experimentally, cerium ions were excited with circularly polarized laser pulses and their fluorescence was detected within the spectral window 485 through 525 nm to ensure that it terminates at one of the $^2F_{5/2}$ sublevels. Its polarization was also chosen to be either σ_+ or σ_-. An external magnetic field was applied either parallel or perpendicular to the excitation beam propagation direction. With the magnetic field being along the excitation beam, the amounts of the fluorescence corresponding to σ_+ and σ_- polarizations significantly differ in the beginning of the decay indicating nonequilibrium populations of $5d(\uparrow)$ and $5d(\downarrow)$ states [see Fig. 3(a)]. The decay traces merge once the populations equilibriate due to spin-flip processes, being most probably related to Orbach or phonon Raman relaxation [14]. The difference between the $5d(\uparrow)$ and $5d(\downarrow)$ decay signals gives the spin-lattice relaxation time $T_1 = 26$ ns [see inset in Fig. 3(a)], which is in agreement with the previously reported value [12]. The calculated electron spin polarization of the excited $5d$ state is 97%; however, the contrast of the corresponding fluorescent signal is partially reduced by decay into the two Kramer's doublets of the $^2F_{5/2}$ manifold elevated above the ground state by 228 and 587 cm^{-1}, respectively, resulting in the ratio of the polarized fluorescence intensities right after the laser pulse $I(\sigma_+)/I(\sigma_-) \approx 2$. This contrast agrees well with the theoretically calculated one [see the Supplemental Material, Fig. S3(a) [9]]. The contrast between σ_+ and σ_- intensities can be completely restored if one detects only the fluorescence corresponding to the ZPL of the cerium ion at low temperature. Furthermore, the fidelity of spin polarization in the excited state can be improved up to 99.7% by directing the excitation beam along the y axis of the local cerium site.

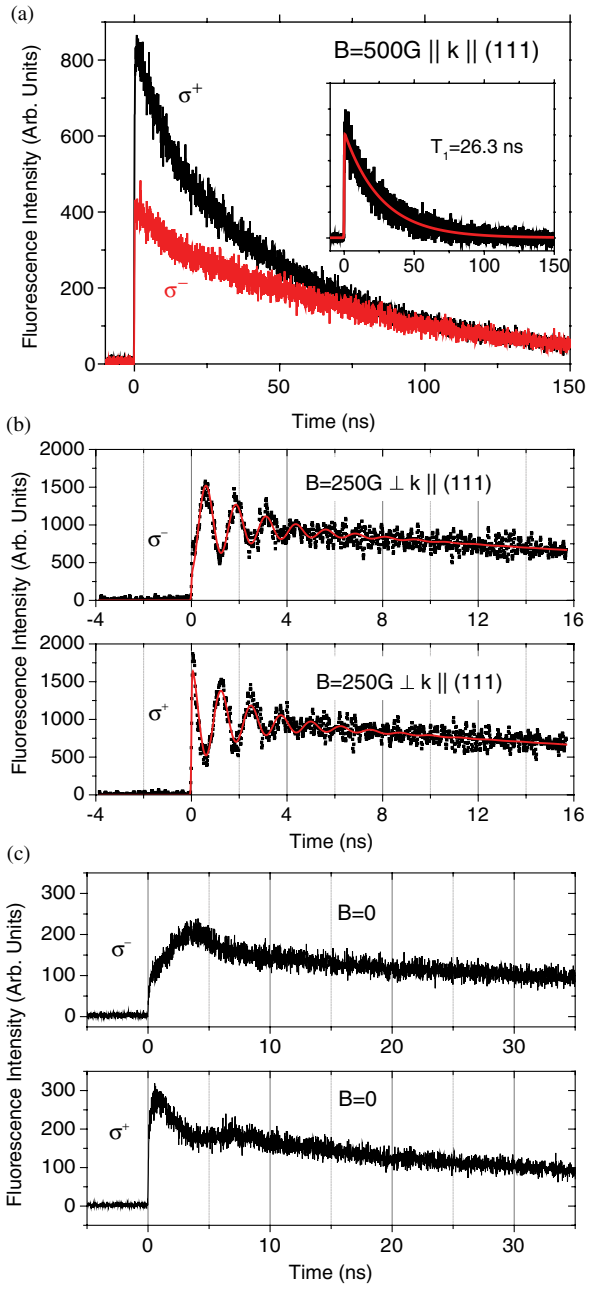

FIG. 3 (color online). Quantum beats of the fluorescence of a single Ce^{3+} ion. Solid lines represent fitting curves. (a) σ_+ and σ_- decay signals after excitation with a circularly polarized laser pulse. The external magnetic field of 500 G is along the laser propagation direction parallel to the (111) crystal axis. (b) Larmor precession of the excited electron spin visualized by oscillating behavior of the σ_+ and σ_--polarized emissions. The magnetic field of 250 G is perpendicular to the (111) crystal axis and to the excitation laser direction. (c) Nonexponential decay of the σ_+ and σ_--polarized fluorescent signals reveals strong hyperfine coupling to the surrounding ^{27}Al nuclei.

In the case of the magnetic field being perpendicular to the excitation beam, rapid out-of-phase oscillations of the σ_+ and σ_- fluorescence signals originating from $5d(\uparrow)$ and $5d(\downarrow)$ states reflect Larmor precession of the electron spin as indicated in Fig. 3(b). The signals were fitted with the decaying cosine function superimposed onto the exponential decay,

$$I_{\pm}(t) = \exp(-t/t_1) \pm a\cos(2\pi\nu t)\exp(-t/t_2). \quad (2)$$

The fit gave an oscillation contrast $a = 0.63$ which is in good agreement with the theoretically predicted contrast of 0.57 for the case of (111) orientation of the crystal (see Supplemental Material [9]). Larmor frequency extracted from the fit is $\nu = 796$ MHz and corresponds to the g factor of 2.2 for the $5d(1)$ state. Finally, the lifetime of the oscillations is found to be 2.2 ns. If no external magnetic field is applied, the σ_+ and σ_- decay signals represent cerium spin precession in the magnetic field produced by the nearby ^{27}Al averaged over all possible configurations of the ^{27}Al nuclear spin bath and show nonexponential behavior [see Fig. 3(c)].

In summary, the detection of individual Ce^{3+} ions in a crystal is confirmed by spectral, lifetime, and photon antibunching measurements. Single cerium ions can be prepared in a well-defined spin state of the lowest $5d$ level by optical pumping with circularly polarized light. The achievable degree of spin polarization depends on the orientation of the cerium center with respect to the excitation propagation direction and can be higher than 99%. The coherent state of the spin can be read out by observing the dynamics of the emitted fluorescence polarization. While the full fidelity of readout can be achieved by observing the temporal dynamics of the polarization of cerium ZPL at low temperature, even room temperature measurements demonstrate clear correlation between the spin state of the emitting level and the polarization of the fluorescene. Cooling the crystal down to cryogenic temperatures would also eliminate fast relaxation in the ground state, thus, opening a possibility of all-optical addressing of cerium spin in the lowest $4f$ state and allowing for single spin optical memory similar to the one previously demonstrated using quantum dots [15]. In turn, optical detection of a single Ce^{3+} ion and study of its magneto-optical properties in low-spin crystal hosts like, for example, yttrium orthosilicate [16] would dramatically increase the decoherence time. Simultaneously, it offers an access to the spin states of individual nuclear spins, ^{29}Si or ^{17}O, through the magnetic hyperfine interaction similar to the case of ^{27}Al nuclei in YAG. Furthermore, optical selection rules corresponding to optical ZPL of cerium would allow one to realize spin-photon entanglement [17] in RE-doped crystalline material. Thus, a combination of atomiclike optical selection rules demonstrated in the present work and potentially long spin memory specific to RE ions trapped in solids make Ce^{3+} an ideal candidate for quantum information processing.

We would like to thank Philip Hemmer for stimulating discussions. The work was financially supported by ERC SQUTEC, SFB TR21, and DFG FOR 1493.

[1] H. Lin, T. Wang, and T. W. Mossberg, Opt. Lett. **20**, 1658 (1995); Y. S. Bai and R. Kachru, Opt. Lett. **18**, 1189 (1993); R. Yano, M. Mitsunaga, and N. Uesugi, J. Opt. Soc. Am. B **9**, 992 (1992).

[2] J. J. Longdell, E. Fraval, M. J. Sellars, and N. B. Manson. Phys. Rev. Lett. **95**, 063601 (2005).

[3] H. de Riedmatten, M. Afzelius, M. U. Staudt, C. Simon, and N. Gisin, Nature (London) **456**, 773 (2008); C. Clausen, F. Bussieres, M. Afzelius, and Nicolas Gisin, Phys. Rev. Lett. **108**, 190503 (2012).

[4] C. Clausen, I. Usmani, F. Bussiéres, N. Sangouard, M. Afzelius, H. de Riedmatten, and N. Gisin, Nature (London) **469**, 508 (2011); E. Saglamyurek, N. Sinclair, J. Jin, J. A. Slater, D. Oblak, F. Bussières, M. George, R. Ricken, W. Sohler, and W. Tittel, Nature (London) **469**, 512 (2011).

[5] J. H. Wesenberg, K. Mølmer, L. Rippe, and S. Kröll, Phys. Rev. A **75**, 012304 (2007); Y. Yan, J. Karlsson, L. Rippe, A. Walther, D. Serrano, D. Lindgren, M. E. Pistol, S. Kröll, P. Goldner, L. Zheng, and J. Xu., Phys. Rev. B **87**, 184205 (2013).

[6] R. Kolesov, K. Xia, R. Reuter, R. Stöhr, A. Zappe, J. Meijer, P. R. Hemmer, and J. Wrachtrup, Nat. Commun. **3**, 1029 (2012).

[7] C. Yin, M. Rancic, G. G. de Boo, N. Stavrias, J. C. McCallum, M. J. Sellars, and S. Rogge, Nature (London) **497**, 91 (2013).

[8] M. J. Weber, Solid State Commun. **12**, 741 (1973).

[9] See Supplemental Material at http://link.aps.org/supplemental/10.1103/PhysRevLett.111.120502 for details on calculation of level structure and optical dipole moments, sketch of the experimental setup, estimate of its light collection efficiency, calculated optical selection rules, and expected shapes of fluorescence signals calculated under experimental conditions.

[10] J. P. van der Ziel, M. D. Sturge, and L. G. Van Uitert, Phys. Rev. Lett. **27**, 508 (1971).

[11] M. Kučera and J. Hakenová, J. Magn. Magn. Mater. **104–107**, 439 (1992).

[12] R. Kolesov, Phys. Rev. A **76**, 043831 (2007).

[13] D. J. Robbins, J. Electrochem. Soc. **126**, 1550 (1979).

[14] R. Orbach, Proc. R. Soc. A **264**, 458 (1961); L. Pidol, O. Guillot-Noël, A. Kahn-Harari, B. Viana, D. Pelenc, and D. Gourier, J. Phys. Chem. Solids **67**, 643 (2006).

[15] M. Kroutvar, Y. Ducommun, D. Heiss, M. Bichler, D. Schuh, G. Abstreiter, and J. J. Finley, Nature (London) **432**, 81 (2004).

[16] S. Saha, P. S. Chowdhury, and A. Patra, J. Phys. Chem. B **109**, 2699 (2005).

[17] B. B. Blinov, D. L. Moehring, L.-M. Duan, and C. Monroe, Nature (London) **428**, 153 (2004); T. Wilk, S. C. Webster, A. Kuhn, and G. Rempe, Science **317**, 488 (2007); E. Togan, Y. Chu, A. S. Trifonov, L. Jiang, J. Maze, L. Childress, M. V. G. Dutt, A. S. Sørensen, P. R. Hemmer, A. S. Zibrov, and M. D. Lukin, Nature (London) **466**, 730 (2010); W. B. Gao, P. Fallahi, E. Togan, J. Miguel-Sanchez, and A. Imamoglu, Nature (London) **491**, 426 (2012).